International Journal of Engineering, Science and Information Technology
Volume 6, No. 1 (2026) pp. 80-87
eISSN: 2775-2674
Website: http://ijesty.org/index.php/ijesty
DOI: https://doi.org/10.52088/ijesty.v6i1.1786
Research Paper, Short Communication, Review, Technical Paper

Finite Element Analysis of Strength Degradation and Interface Behavior Controlling Bund Wall Stability in an Ex-Mining Pit

Revia Oktaviani[1]*, Tommy Trides[1], Albertus Juvensius Pontus[1], Afdal Jamil Tanjung[1], Haviluddin[2]

[1]Department of Mining Engineering, Faculty of Engineering, Universitas Mulawarman, Samarinda, Indonesia
[2]Department of Informatics, Faculty of Engineering, Universitas Mulawarman, Samarinda, Indonesia

**Corresponding author Email: revia.oktaviani@gmail.com*

The manuscript was received on 11 May 2025, revised on 29 August 2025, and accepted on 29 December 2025, date of publication 21 January 2026

Abstract

This study aims to develop and evaluate a deep learning-based mobile application for the automated classification of ornamental plants, addressing challenges associated with visual similarity among species and environmental variability during image acquisition. The proposed system utilizes a Convolutional Neural Network (CNN) based on the MobileNetV2 architecture, selected for its lightweight structure and deployment efficiency on resource-constrained mobile devices. The dataset comprises approximately 600 images representing 10 ornamental plant classes, collected from real-world environments, and processed through a standardized preprocessing pipeline. Model training was conducted using the Teachable Machine platform over 100 epochs, with a batch size of 16 and a learning rate of 0.001, allocating 90% of the dataset for training and 10% for testing. Experimental results indicate that the proposed model achieves a classification accuracy of 96.3%, corroborated by evaluation metrics including accuracy curves, loss convergence, and class-wise performance analysis. The trained model was successfully converted into a lightweight format and integrated into an Android-based mobile application developed using the Flutter framework. Functional testing demonstrates that the application performs effectively in real-time classification scenarios, maintaining high accuracy and responsive on-device inference without relying on cloud computing. In conclusion, this study confirms that lightweight deep learning architectures, such as MobileNetV2, can be effectively implemented in mobile environments for ornamental plant classification. The proposed application enhances accessibility and usability, enabling rapid and accurate plant identification. Furthermore, this approach contributes to practical applications in horticulture, education, and biodiversity awareness, while demonstrating the feasibility of deploying efficient deep learning models on mobile platforms.

Keywords: *Deep Learning, Convolutional Neural Network, Mobile Application, Plant Classification.*

1. Introduction

Open pit coal mining generates substantial overburden requiring safety in pit placement to maintain operational and environmental security. One increasingly adopted strategy is constructing in mine embankments, where waste is deposited inside the mined-out void to form bund walls that function as engineered barriers against lateral deformation and erosion [1]. Their performance, however, is highly sensitive to rainfall, foundation conditions, and material softening factors that are especially critical in tropical mines.

A failure case at Pit Banda demonstrated how intense rainfall infiltration increased pore pressure, reduced strength, and triggered lateral spreading of a temporary coal bund wall. Similar rainfall-induced instabilities have been widely reported in open pit and embankment systems [2], [3], underscoring the need for numerical approaches capable of capturing hydromechanical responses in heterogeneous soils. While Limit Equilibrium Methods remain common, Finite Element Method (FEM) modeling provides a more rigorous evaluation of deformation and progressive failure in large embankments [4], curved geometries [5], and saturated soils under rainfall or seismic loading [6], [7]. Accordingly, this study applies FEM-based Phase2 with Strength Reduction Technique (SRT) for stability assessment [8], [9].

The novelty of this research lies in modeling a 75 m high arched permanent bund wall in an ex-mining pit under equatorial conditions, incorporating cohesion-loss scenarios of 0%, 25%, and 50% to simulate rainfall induced degradation across three critical zones: the bund wall slope, transition layer, and siltstone foundation. The findings provide new insights for safer bund wall design in high rainfall mining environments.

2. Methods

The embankment materials soft clay, sandy clay, and loose sand are controlled by the complex geology of the Tarakan Basin, comprising the Birang, Latih, Labanan, and Sinjin Formations [10]. Primary data were collected through field sampling at the Banda Pit, including overburden for bund wall construction, rock samples representing the siltstone foundation, and mud samples to simulate retained load conditions. Laboratory testing following ASTM standards determined density, permeability, Atterberg limits, cohesion, and internal friction angle as input parameters for numerical analysis.

A quantitative approach was applied, combining laboratory data with Finite Element Method (FEM) simulations to evaluate slope stability. FEM was selected over Limit Equilibrium Methods due to its superior ability to represent stress-strain behavior and complex failure mechanisms in embankments, as demonstrated by Jian & Deng [9]. The method discretizes the slope into finite elements and computes nodal displacements through interpolation. Phase2 software was used to model the bund wall behavior using the Shear Strength Reduction (SSR) technique, where shear parameters cohesion (c) and internal friction angle (ϕ) are progressively reduced by a Strength Reduction Factor (SRF) until the onset of failure [11]. The reduced parameters at each step are given by:

$$c_r = \frac{c}{SRF} \quad , \quad tan_r = \frac{tan}{SRF} \tag{1}$$

$$\tau_r = \frac{c}{SRF} + \sigma = \frac{c + \sigma\ tan}{SRF} \tag{2}$$

Bund wall stability was evaluated using FEM with the Shear Strength Reduction (SSR) method [12], where the SRF at numerical failure represents the Factor of Safety (FoS). Six field based cross sections were modeled to assess deformation and failure mechanisms under reduced shear strength. The base layer was analyzed for settlement under overburden loading, while the siltstone foundation was checked for bearing failure, with ultimate bearing capacity (qu) estimated using Terzaghi's equation.

$$q_u = cN_c + qN_q + 0.5\gamma BN_\gamma \tag{3}$$

Where q_u is ultimate bearing capacity, c is cohesion, q is surcharge, γ is unit weight, B is foundation width, and N_c, N_q, N_γ are bearing capacity factors dependent on internal friction angle (ϕ). The net allowable bearing capacity ($q_{a,net}$) was calculated as:

$$q_{a,net} = \frac{q_u - q}{FS} \tag{4}$$

Where FS is Factor of Safety. Foundation–sidewall interaction was also modeled to evaluate the effect of lateral stress resulting from mud accumulation and water saturation on slope integrity. To account for seismic loading and its interaction with pore water pressure, the simulations incorporated pseudo-static conditions following Gao et al. [13], using a horizontal seismic coefficient k_h= 0.05g, which reflects the low regional seismicity of East Kalimantan, Indonesia [14]. The pseudo-static load was calculated as:

$$F_s = k_h.W \tag{5}$$

where F_s is horizontal inertial force and W is the weight of soil or waste. Following Wyllie & Mah [15], a Factor of Safety above 1,1 was targeted for dynamic conditions

3. Results and Discussion

In the Banda Pit area, coal material was previously used as a temporary retaining wall. However, in June 2024, heavy rainfall (185.6-222.2 mm) triggered significant movement of saturated mud, increasing lateral earth pressure beyond the structure's design capacity and causing slope failure (Figure 1).

The failure sequence highlights the risks of using low-cohesion coal as a structural element under extreme hydrological stress. Early indicators of instability (Figure 1a), including peak cracking and deformation, resulted from tensile strain, differential settlement, and rising pore water pressure from rainfall infiltration. Similar hydrologically driven failures have been reported in mining waste dumps, where real-time infiltration altered pore pressure and reduced shear strength [16]. Continuous rainfall rapidly saturated the coal and underlying seams, further decreasing strength, especially in poorly drained zones.

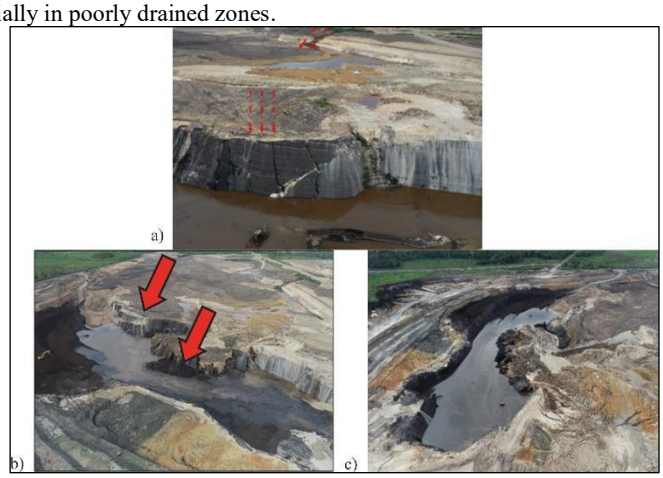

Fig 1. a) Conditions before landslide in the in-pit dam; b) and c) Conditions after the landslide in the in-pit dam

Post-failure conditions (Figures 1b and 1c) show major changes in slope geometry, with displaced material forming a new failure surface marked by both shallow and deep movement. To prevent additional displacement from running off and mass movement, a permanent bund wall was proposed inside the pit. This structure is intended to resist lateral and gravitational forces and to restore long term stability under hydrologic and mining induced loading aligning with international safety standards for high rainfall tropical mines. The complexity of the post failure geometry and the design requirements for the permanent bund wall necessitate numerical modeling to achieve accurate stability evaluation [17].

3.1. Rock Quality

Geotechnical drilling (GT-02 R) identified three main lithologic units along the depth profile. At depths of 1.6 to 8.8 meters, the unit is characterized by dark gray soft clay, with a Geological Strength Index (IGSI) of 0 to 20 and a RQD between 0% and 51%, indicating very poor to moderate rock mass quality [18][19].
A reddish sandy clay unit was identified at depths of 8.8 to 15.75 meters. GSI values ranged more widely, from 0 to 65, and RQD values ranged from 0% to 100%, indicating poor to very good rock mass quality [20], [21]. The lowest rock unit extending from a depth of 15.75 meters to 48.1 meters is the Coal Seam, with GSI values between 75 and 85, and RQD ranging from 62.5% to 100%, which is classified as fair to very good.

3.2. Physical Properties and Mechanical Properties

Atterberg limit tests were conducted on soft clay, sandy clay 1, and sandy clay 2 to evaluate phase conditions and plasticity. Table 1 shows that the moisture content of the soft clay is close to its liquid limit, implying near liquid phase conditions and an increased risk of instability under loading, especially considering the effects of rainfall infiltration and subsequent time dependent softening [7][22].

Table 1. Plasticity Index Test

No	Material Type	Liquid Limit (%)	Plastic Limit (%)	Plasticity Index (%)	Saturated Density (kN/m^3)
1	Soft clay	49.09	20.24	28.67	15.21
2	Sandy clay 1	55	25.1	29.9	17.46
3	Sandy clay 2	81	35.3	45.7	16.28
4	Disposal	54	37.5	16.5	16.5
5	Mudstone	51	31.2	19.8	11.5
6	Siltstone				20.01
7	Claystone				20.005
	Clay	High Plasticity			

The consistency of fine-grained soils governs their resistance to external forces through clay particle interactions, which control deformation behavior [23]. High plasticity soils typically exhibit low shear strength and significant moisture induced volume change, resulting in poor bearing performance [24]. Clay activity in the Banda Pit ranges from 0.60-0.89, indicating moderate reactivity. Based on the criteria proposed by Skempton and Mitchell and Soga, the dominant clay minerals illite, kaolinite, attapulgite, and allophane are associated with the low to moderate expansion zone in the plasticity index clay content chart proposed by Seed *et al.*, suggesting relatively stable volumetric behavior suitable for bund wall construction [25]-[27]. Direct shear testing of these materials provided shear strength parameters, cohesion (c) and internal friction angle (ϕ), which form the primary geotechnical inputs for the stability analysis of all bund wall components.

Table 2. Mechanical Properties Test Results

No	Material Type	Mechanical Properties			
		Direct Shear Test		Elastic Modulus (kN/m^2)	Poison Ratio
		c (kN/m^2)	φ (^{0})		
1	Disposal	42.46	15.22	276000	0.3
2	Mud stone	35.81	20.69	250000	0.3
3	Sandy clay	40.93	34.81	276000	0.25
4	Coal	48.88	30.05	170870	0.17
5	Claystone	49.46	25.29	47197.5	0.30
6	Siltstone	55.7	23.99	45830	0.25

3.3. Bund wall stability analysis

The embankment wall design, shown in Figure 2, has an overall height of 75 meters and a base width of approximately 130 meters. Its geometry consists of individual slope segments with a height of 5 meters, a slope angle of 43°, and an embankment with an average width of 5 meters. The embankment wall is shaped in a curved configuration, forming a horizontal curve with a central angle of 52°.

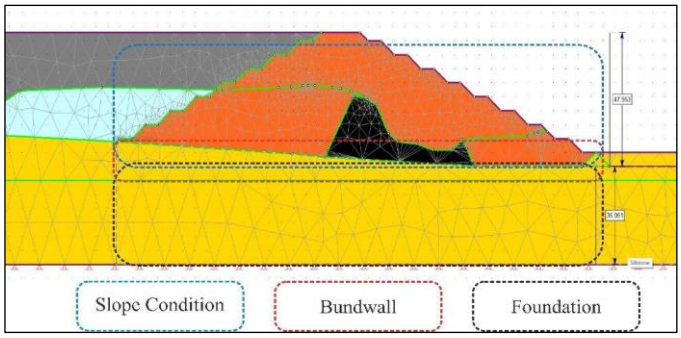

Fig 2. Bund wall design

Stability analysis was conducted in six cross sections (Sections 1-6, Figure 3), each divided into three zones: the slope face, embankment base, and foundation interface. The sections were selected to capture geometric and loading variations along the bund wall, focusing on areas prone to differential settlement or increased overburden pressure, while accounting for interactions between compacted fill and in situ subgrade and the anisotropic stress redistribution induced by the wall's curved alignment.

Using a Finite Element Method (FEM) based approach, slope simulations were performed at three cohesion reduction conditions: 0%, 25%, and 50%, indicating progressive softening of the embankment material. This sensitivity analysis reflects the seasonal humidity variations common in tropical climates such as East Kalimantan, with high rainfall during the rainy season and high temperatures (33°C to 37°C) during the dry season, which can potentially lead to a decrease in material strength.

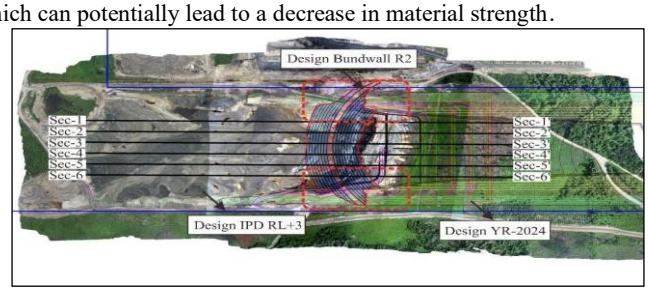

Fig 3. Bund wall with six cross-sections

3.3.1. Slope stability analysis of bund wall

The sandy clay overburden selected for the bund wall has a dry unit weight of 20.01 kN/m³ and reaches maximum dry density at 21% optimum water content, indicating good compaction potential and adequate shear resistance. A CBR value obtained at 13.88% moisture representative of dry season field conditions confirms sufficient bearing capacity and highlights the need for strict moisture control during placement. The bund wall is designed with a 5 m bench at 43° and an overall height of 48 m at 25°, incorporating 0.05 g seismic loading. FEM based stability analysis across six cross sections yields a representative FoS of 1.87 at Section 3–3' under 50% cohesion reduction. Table 3 shows a consistent decrease in Dynamic FoS with cohesion loss: from 2.34 - 2.55 at intact cohesion to 2.15 - 2.27 at 75% reduction. The lowest stability occurs at 50% cohesion, where Sections 3-3' (see Figure 4) and 4-4' both reach FoS = 1.87, indicating the central bund wall zone as the most vulnerable. These results underscore that cohesion governs dynamic stability and that rigorous engineering control particularly compaction quality, is critical for sandy clay filling in bund wall construction.

Table 3. Dynamic Factor of Safety of Bund wall Slope

No	Analysis	Dynamic Factor of Safety		
		*100%	*75%	*50%
1	Section 1-1'	2.41	2.18	1.95
2	Section 2-2'	2.47	2.18	1.92
3	Section 3-3'	2.34	2.15	1.87
4	Section 4-4'	2.45	2.17	1.87
5	Section 5-5'	2.44	2.22	1.96
6	Section 6-6'	2.55	2.27	1.98

* Decrease in bund wall material cohesion value

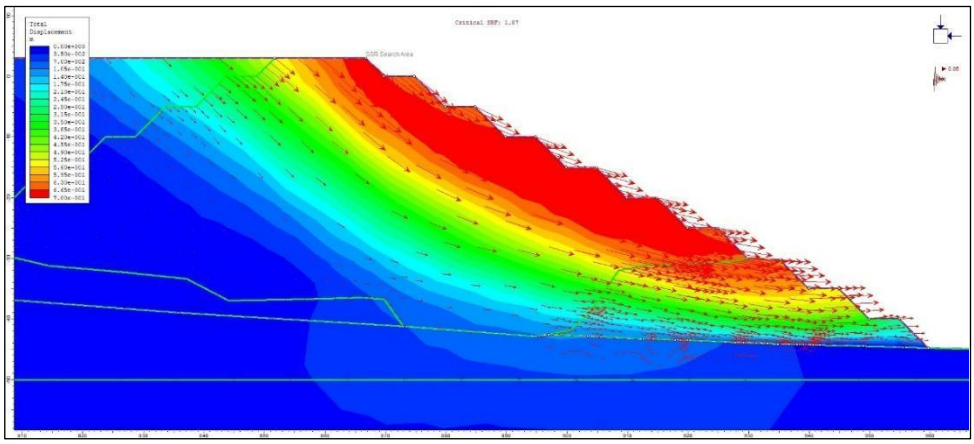

Fig 4. Dynamic Factor of Safety of Bund wall Slope section 3-3'

3.3.2. Bund wall base stability analysis

A stability analysis was conducted for the transitional base layer above the bund wall foundation, which functions as a stress redistributing medium between the wall body and subgrade. Although not a structural foundation, instability in this layer could mobilize lateral displacement of the entire bund wall under mudstone loading, making its mechanical performance critical.

Sandy clay was selected due to its cohesion potential, supported by compaction parameters of ω_{opt} = 22.26% and γ_d = 1.87 kN/m³. FEM simulations were performed under three cohesion scenarios (100%, 75%, 50%) to evaluate settlement, consolidation, and shear resistance. Dynamic Factors of Safety (FoS) from six cross sections demonstrate the material's sensitivity to cohesion reduction. At 100% cohesion, FoS values range from 5.33-5.81, exceeding recommended limits for static (1.5) and dynamic (1.1) stability. Even with 50% cohesion loss, all sections remain above threshold values, confirming strong basal stability (Tabel 4). However, a consistent decline in FoS indicates vulnerability to shear-strength degradation. Sections 3-3' and 4-4' show the lowest FoS under the weakest scenario (3.40 and 3.45), identifying them as priority monitoring zones during operation as softening increases.

Table 4. Bund wall Base Slope Dynamic Factor of Safety

No	Analysis	Bund wall Base Slope Dynamic Factor of Safety		
		*100%	*75%	*50%
1	Section 1-1'	5.59	4.92	3.75
2	Section 2-2'	5.81	4.73	3.71
3	Section 3-3'	5.32	4.18	3.4
4	Section 4-4'	5.54	4.51	3.45
5	Section 5-5'	5.63	4.48	3.46
6	Section 6-6'	5.66	4.63	3.61

The bund wall will transfer all structural loads to the bedrock. In this study, the bund wall was constructed on a layer of siltstone that resisted vertical stresses from the embankment and lateral forces from mud and water. This analysis examined vertical failure modes, specifically support failure due to increased loading. Although shear strength in the siltstone could cause settlement or displacement, simulation results indicate that the factor of safety remained well above the required limit. Even with a 50% reduction in cohesion, the siltstone maintained a high bearing capacity, demonstrating its robustness in supporting a large bund wall.

Dynamic loading (0.05 g) produced negligible effects, indicating sufficient stiffness and shear strength of the siltstone to prevent vertical deformation or shear failure. Section 4-4' (Figure 5) recorded the lowest FoS (8.01), which remained unchanged despite the reduction in strength, attributed to the thicker siltstone layer and uniform load distribution. In comparison, the FoS at the base of the bund wall ranged from 3.4 to 5.8 (Table 5), indicating lower stability compared to the foundation. Therefore, the primary focus shifted from the foundation to the transitional base layer, where the influence of the mud and varying strengths increased the likelihood of instability.

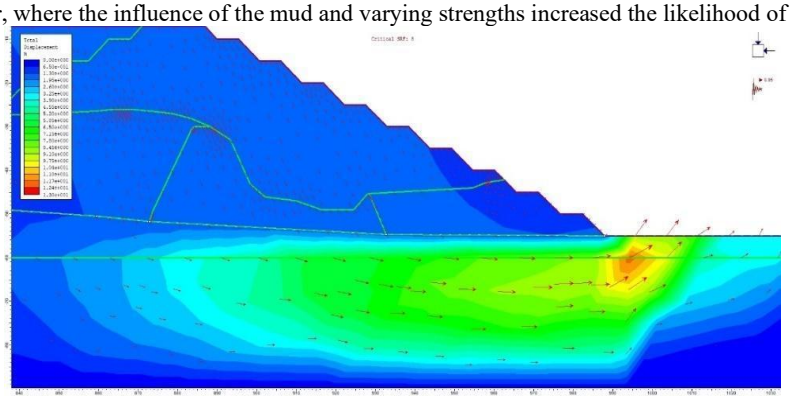

Fig 5. Bund wall Foundation Stability Analysis Section 1-1'

Table 5. Bund wall foundation dynamic Factor of Safety

No	Analysis	Bund wall foundation dynamic Factor of Safety		
		*100%	*75%	*50%
1	Section 1-1'	8	8	8.01
2	Section 2-2'	8.15	8.2	8.15
3	Section 3-3'	8.26	8.25	8.25
4	Section 4-4'	9.6	9.99	9.69
5	Section 5-5'	10.27	10.27	10.27
6	Section 6-6'	8.74	8.65	8.91

3.4. Factor of safety analysis at the sidewall–bund wall interface

The interaction between the bund wall and adjacent sidewalls was assessed by examining the vertical (σ_z) and horizontal stress distributions with depth to determine the factor of safety and potential interface failure mechanisms. Stability at various elevations and contact angles was evaluated using the Safety Reduction Factor (SRF). Table 6 (depth -35 m) highlights two key trends governing the mechanical behavior of the bund wall sidewall system.

Figure 6 presents stress simulations from a depth of 0 to -35 m, incorporating a bulk unit weight of 11.5 kN/m³ for the upper layer (0 to -15 m) and 16.5 kN/m³ below 20 m. The increase in σ_z reflects the combined effect of the self-weight and applied load. At a depth of -35 m, the vertical stress reached 577.50 kN/m², while the horizontal stress was 84.15 kN/m², indicating significant lateral pressure at the interface. These values serve as boundary inputs in FEM modeling to evaluate slope stability and failure risk. This stress behavior is important for understanding load transfer, shear response, and the potential development of failure surfaces or arching effects along the bund sidewall interface.

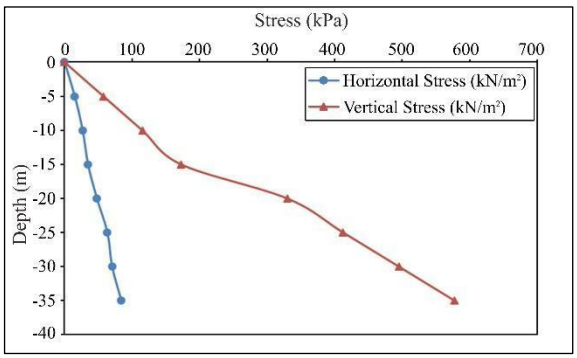

Fig 6. Stress Distribution Sidewall-Bund wall Interface

Table 6. Safety Reduction Factor (SRF) as a measure of slope stability

No.	Depth (m)	Sudut Kontak (^{0})	SRF
1	- 5	52	3.1
2	-10	57	2.31
3	-15	62	2.29
4	-20	64	2.03
5	-25	64	1.72
6	-30	67	1.76
7	-35	67	1.61

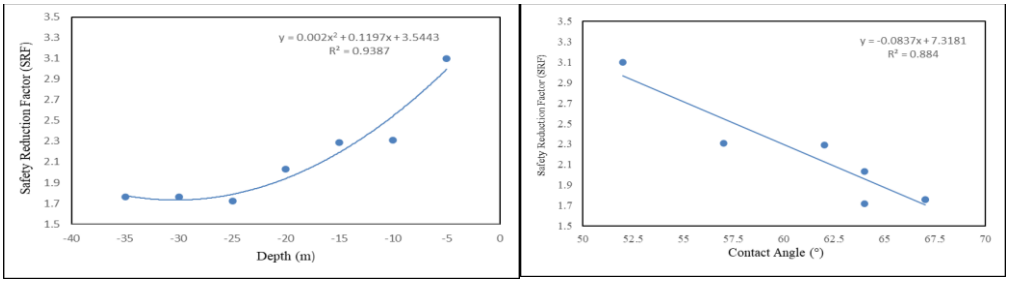

Fig 7. a) Relationship of Safety Reduction Factor (SRF) to Depth; b) Relationship of Safety Reduction Factor (SRF) to Contact Angle

Figure 7a shows a strong quadratic relationship between depth and slope reliability factor (SRF) with an R^2 value of 0.9387, allowing prediction of critical depths using the equation $y = 0.002x^2 + 0.1197x + 3.5443$. The SRF decreases below 2.0 at depths greater than -25 m, approaching the minimum temporary stability criterion of FoS ≥ 1.5, indicating potential structural vulnerability near the base of the bund wall [28], [29]. Figure 7b reveals an inverse linear correlation between contact angle and SRF ($R^2 = 0.884$), where increasing interface inclination reduces stability and may promote planar or translational failure mechanisms [15]. Overall, slope design must account not only for material strength but also for geometric configuration and interface behavior under increasing dump height [12][30].

4. Conclusion

The bund wall demonstrates stable performance, with slope Factors of Safety (1.87-2.55) remaining above the minimum pseudo-static criteria even under a 50% cohesion reduction. The compacted sandy clay base shows high stability (FoS 3.40-5.81), while the siltstone foundation provides exceptional bearing capacity (FoS 7.79-10.27), indicating negligible settlement risk. Critical zones occur in Sections 3-3', 4-4', and along the sidewall bund wall interface below 25 m, where SRF values approach 1.76, reflecting heightened sensitivity to stress concentration and strength loss. Overall, the bund wall system is structurally robust; however, strict compaction control, focused monitoring of central sections, and reliable drainage maintenance are essential to mitigate risks associated with saturation and long-term material degradation.

Acknowledgement

This research was funded by the Faculty of Engineering, Mulawarman University through the Tropical Engineering Program 2025. The authors express sincere gratitude for the financial support provided. The authors wish to thank Mr Jatmiko and Mr Sriwijayanto W. for the opportunity to address the in-pit dump case study. We also appreciate Prof. Rahman Thamrin for supplying the drilling equipment and crew for rock sampling, and Mr Winarno Agus for his assistance during laboratory testing.

References

[1] B. H. G. Brady and E. T. Brown, *Rock Mechanics for Underground Mining*. Springer, 2006.
[2] X. Guo, Y. Wang, Y. Jiang, and Q. Liu, "Failure mechanism of soil slopes under heavy rainfall in tropical and subtropical regions," *Catena*, vol. 200, Art. no. 105151, 2021.
[3] M. Zhang, H. Cheng, W. Wang, and R. Wei, "Probabilistic stability assessment of retaining structures in tropical residual soil under varied rainfall infiltration," *Soils Found.*, vol. 64, no. 1, Art. no. 101416, 2024.
[4] D. Li, G. Chen, Q. Xu, and L. Zhang, "Three-dimensional numerical analysis of dump slope stability in large open-pit mines," *Int. J. Min. Sci. Technol.*, vol. 31, no. 2, pp. 183–193, 2021.
[5] J. Luo, C. Zhang, S. Li, and H. Li, "Stability evaluation of earth dams with curved alignment using the strength reduction finite element method," *Comput. Geotech.*, vol. 146, Art. no. 104710, 2022.
[6] X. Zhang, Y. Wang, L. Zhang, and Z. Li, "Stability analysis of high and steep slopes under rainfall and seismic conditions: A comparative study of LEM and FEM," *Eng. Geol.*, vol. 314, Art. no. 107000, 2023.
[7] H. Sun, H. Yang, B. Xu, and Z. Zhang, "Time-dependent stability analysis of high-plasticity clay slopes considering rainfall infiltration and softening," *Geosciences*, vol. 13, no. 11, Art. no. 327, 2023.
[8] J. Huang, X. Li, Y. Wang, and R. Wei, "A new strength reduction method for slope stability analysis based on the stress state variable," *Int. J. Numer. Anal. Methods Geomech.*, vol. 46, no. 9, pp. 1659–1678, 2022.
[9] Y. Jian and T. Deng, "Comparative study on stability of tailings dam slopes based on limit equilibrium and finite element methods," *J. Geotech. Geoenviron. Eng.*, vol. 150, no. 4, Art. no. 04024003, 2024.
[10] B. Situmorang and F. Burhan, *Peta Geologi Lembar Tanjung Redeb*. Bandung, Indonesia: Pusat Survei Geologi, 2011.
[11] E. M. Dawson, W. H. Roth, and A. Drescher, "Slope stability analysis by strength reduction," *Géotechnique*, vol. 49, no. 6, pp. 835–840, 1999.
[12] D. V. Griffiths and P. A. Lane, "Slope stability analysis by finite elements," *Géotechnique*, vol. 49, no. 3, pp. 387–403, 1999.
[13] S. Gao, J. Zhang, and Y. Li, "Seismic stability analysis of a high mine dump considering the effect of pore water pressure," *J. Rock Mech. Geotech. Eng.*, vol. 12, no. 5, pp. 1004–1015, 2020.
[14] Transportation Research Board, *Seismic Analysis and Design of Retaining Walls, Buried Structures, Slopes, and Embankments – Volume 1*, NCHRP Report 611, Washington, D.C., USA, 2008.
[15] D. C. Wyllie and C. W. Mah, *Rock Slope Engineering: Civil and Mining*, 4th ed. London, UK: Spon Press, 2004.
[16] J. R. Pérez-López and J. Garzón-Roca, "Advanced stability analysis of mining waste dumps incorporating real-time hydrological data," *Minerals*, vol. 12, no. 8, Art. no. 953, 2022.
[17] K. Yang, M. Deng, and W. Wang, "Stability analysis of slopes with complex structures using the numerical manifold method," *Rock Mech. Rock Eng.*, vol. 57, pp. 2099–2118, 2024.
[18] Z. T. Bieniawski, *Engineering Rock Mass Classifications: A Complete Manual for Engineers and Geologists in Mining, Civil, and Petroleum Engineering*. New York, NY, USA: John Wiley & Sons, Inc., 1989.
[19] A. Palmström and E. Broch, "Use and misuse of rock mass classification systems with particular reference to the Q-system," *Tunn. Undergr. Space Technol.*, vol. 21, no. 6, pp. 575–593, 2006.
[20] ISRM, *Rock Characterization, Testing and Monitoring: ISRM Suggested Methods*, E. T. Brown, Ed. Oxford, UK: Pergamon Press, 1981.
[21] E. Hoek and E. T. Brown, "Practical estimates of rock mass strength," *Int. J. Rock Mech. Min. Sci.*, vol. 34, no. 8, pp. 1165–1186, 1997.
[22] ASTM, *Standard Test Methods for Liquid Limit, Plastic Limit, and Plasticity Index of Soils*, ASTM Standard D4318, ASTM International, West Conshohocken, PA, 2017.
[23] B. M. Das, *Principles of Geotechnical Engineering*, 6th ed. Stamford, CT, USA: Cengage Learning, 2007.

[24] R. D. Holtz, W. D. Kovacs, and T. C. Sheahan, *An Introduction to Geotechnical Engineering*, 2nd ed. Upper Saddle River, NJ, USA: Pearson, 2011.
[25] A. W. Skempton, "The colloidal activity of clays," *Géotechnique*, vol. 3, no. 1, pp. 30–53, 1953.
[26] J. K. Mitchell and K. Soga, *Fundamentals of Soil Behavior*, 3rd ed. Hoboken, NJ, USA: John Wiley & Sons, Inc., 2005.
[27] H. B. Seed, R. J. Woodward, and R. Lundgren, "Prediction of swelling potential for compacted clays," *J. Soil Mech. Found. Div.*, vol. 88, no. 3, pp. 53–87, 1962.
[28] J. M. Duncan, S. G. Wright, and T. L. Brandon, *Soil Strength and Slope Stability*, 2nd ed. Hoboken, NJ, USA: John Wiley & Sons, Inc., 2014.
[29] E. Hoek and J. W. Bray, *Rock Slope Engineering*, 3rd ed. London, UK: The Institution of Mining and Metallurgy, 1981.
[30] S. Chen, Y. Li, and G. Wang, "Numerical modeling of embankment failure due to basal sliding on soft clay foundations," *Can. Geotech. J.*, vol. 60, no. 11, pp. 1662–1678, 2023.